

A 3D hypoplastic model for cyclic analysis of concrete structures

Toader A. Balan ^a, Enrico Spacone ^{b,*}, Minh Kwon ^b

^a Applied Science Division, Weidlinger Associates, Inc., Los Altos, CA 94022, USA

^b Department of Civil, Environmental and Architectural Engineering, University of Colorado, Boulder, 80309-0428, USA

Received 13 October 1999; received in revised form 27 April 2000; accepted 27 April 2000

Abstract

This paper presents a hypoplastic model for three-dimensional analysis of concrete structures under monotonic, cyclic, proportional and non-proportional loading. The constitutive model is based on the concept of equivalent uniaxial strains that allow the assumed orthotropic model to be described via three equivalent uniaxial stress–strain curves. The characteristics of these curves are obtained from the ultimate strength surface in the principal stress space based on the Willam–Warnke curve. A cap model is added to consider loading along or near the hydrostatic axis. The equivalent uniaxial curve is based on the Popovics and Saenz models. The post-peak behavior is adjusted to account for the effects of confinement and to describe the change in response from brittle to ductile as the lateral confinement increases. Correlation studies with available experimental tests are presented to demonstrate the model performance. Tests with monotonic loading on specimens under constant lateral confinement are considered first, followed by biaxial and triaxial tests with cyclic loads. The triaxial test example considers non-proportional loading. © 2000 Elsevier Science Ltd. All rights reserved.

Keywords: Constitutive model; Finite element analysis; Concrete; Hypoplastic model; Orthotropic model; Equivalent uniaxial strain

1. Introduction

Concrete is a non-homogeneous, anisotropic material whose response is nonlinear even under small stress levels. Furthermore, concrete exhibits a different behavior under tension and compression stresses. In compression, the response hardens up to a peak stress value that depends on the level of lateral confinement. The post-peak behavior depends in general on the level of lateral confinement [18]. Under low confinement, the post-peak response is brittle softening. For increasing confinement stresses, the response of concrete changes to ductile hardening [10,18]. Under tensile stresses, concrete cracks and eventually loses strength entirely.

Experimental test programs have been conducted to study the behavior of concrete under triaxial states of stresses [8,9,12,17,20,22]. These tests are difficult to perform because of the generally unstable response of the specimens near or after the peak. Displacement-con-

trolled tests are used to partially circumvent this problem. Furthermore, because of the concrete sensitivity to the lateral confinement, the response of the cylindrical specimens typically used in tests is highly dependent on the restraint conditions at the end faces.

The response of concrete to triaxial states of stress greatly depends on the formation and expansion of microcracks [22]. Several test programs have shown that the evolution of the microcracks governs the concrete brittleness, ductility, dilatancy and failure modes. All these phenomena depend in general on the triaxial state of stress applied to the concrete. Under low lateral confinement, the failure mode observed in uniaxial compression tests is caused by vertical tension splitting. A sharp post peak loss of strength is observed. Under gradually larger confinement, cracking and damage become more distributed and concrete becomes ductile, with little or no post-peak degradation.

The complex nonlinear behavior of concrete makes it a difficult material to model. In spite of the widespread interest in modeling of concrete under three-dimensional states of stresses, few models are available for immediate and simple numerical implementation in finite element codes. Models developed to date range from

* Corresponding author. Tel.: +1-303-492-7607; fax: +1-303-492-7317.

E-mail address: spacone@colorado.edu (E. Spacone).

very sophisticated laws based on plasticity theory that rely on the definition of a plastic flow rule and on the separation of the deformation increments into plastic and elastic components, to simpler models based on phenomenological rules. The concrete models proposed to date include laws based on nonlinear elasticity, plasticity, endochronic plasticity, microplane theory, damage and fracture mechanics, just to cite a few examples.

The application of the concrete constitutive law to the 3D finite element analysis of concrete and reinforced concrete structural elements and subassemblages necessitates the availability of models that are both mechanically justified and computationally robust. Models should be able to simulate the most important characteristics of the monotonic and cyclic response of concrete under triaxial states of stresses, while maintaining a certain computational simplicity to allow analyses of structural elements with reasonable computational efforts. These requirements have led the authors to the development of a 3D model that relies on the concept of equivalent uniaxial strains. The proposed model is orthotropic, with the axes of orthotropy parallel to the principal stress axes. The model has also been called hypoplastic, from the definition given by Kolymbas [11].

2. 3D concrete model

It is commonly accepted that concrete can be modeled as an initially isotropic material with stress-induced anisotropy. The proposed 3D constitutive law uses an orthotropic model with the axes of orthotropy parallel to the principal stress directions. Principal strain and principal stress directions are not coaxial. The model is based on the concept of equivalent uniaxial strains introduced by Darwin and Pecknold [6], Bashur and Darwin [2] and Elwi and Murray [7]. With respect to the orthotropic axes the incremental constitutive equation is written:

$$d\sigma = C_0 d\varepsilon \quad (1)$$

where $d\sigma$ and $d\varepsilon$ are the stress and strain increments, respectively, and C_0 is the following material matrix:

$$C_0 \quad (2)$$

$$= \frac{1}{\Omega} \begin{bmatrix} E_1(1-v_{23}v_{32}) & E_1(v_{21}+v_{23}v_{31}) & E_1(v_{31}+v_{21}v_{32}) & 0 & 0 & 0 \\ E_2(v_{12}+v_{13}v_{32}) & E_2(1-v_{13}v_{31}) & E_2(v_{32}+v_{12}v_{31}) & 0 & 0 & 0 \\ E_3(v_{13}+v_{12}v_{23}) & E_3(v_{23}+v_{13}v_{21}) & E_3(1-v_{12}v_{21}) & 0 & 0 & 0 \\ 0 & 0 & 0 & G_{12}\Omega & 0 & 0 \\ 0 & 0 & 0 & 0 & G_{23}\Omega & 0 \\ 0 & 0 & 0 & 0 & 0 & G_{31}\Omega \end{bmatrix}$$

where v_{ij} is the transverse strain ratio for strain in the j direction caused by stress in the i direction ($i, j=1, 2, 3$); $\Omega=1-v_{21}v_{12}-v_{31}v_{13}-v_{32}v_{23}-v_{12}v_{23}v_{31}-v_{21}v_{32}v_{13}$; E_i is the material modulus in the i direction of orthotropy ($i=1, 2, 3$); and G_{ij} is the shear modulus in the i - j plane.

Because the shear moduli G_{ij} ($i, j=1, 2, 3$) must be invariant under an arbitrary coordinate transformation of the reference system, Lekhnitskii [13] has shown that the shear moduli are:

$$G_{ij} = \frac{E_i E_j}{E_i(1+v_{ij})+E_j(1+v_{ji})} \quad (3)$$

In a finite element setting, the incremental stress-strain relation with respect to the orthotropic axes must be rotated into the global reference system. This is done by using the rotation matrix \mathbf{T} that contains the direction cosines of the orthotropic axes with respect to the global reference system:

$$\mathbf{C} = \mathbf{T}^T \mathbf{C}_0 \mathbf{T} \quad (4)$$

where \mathbf{C} is the material matrix in the global reference system.

3. Equivalent uniaxial strain

The equivalent uniaxial strain is a fictitious strain with no precise material meaning. It is used to de-couple the 3D material response into three uniaxial constitutive laws. Darwin and Pecknold [6] first introduced the concept. For given principal stresses σ_{p_i} , the equivalent uniaxial strains ε_{ui} are the strains that would induce the same stresses on the equivalent uniaxial stress-strain curves. The material parameters that define the equivalent uniaxial stress-strain curves depend on the current stress ratio, as discussed later in the paper. The equivalent uniaxial strains ε_{ui} are typically derived from the following incremental law:

$$d\varepsilon_{ui} = \frac{d\sigma_{p_i}}{E_i} \quad (5)$$

where $d\sigma_{p_i}$ are the increments of the principal stresses and E_i is the material modulus. The above incremental relation can be written in terms of total increments (E_i is the secant modulus), step increments (E_i is the incremental secant modulus), or infinitesimal increments (E_i is the tangent modulus). In the current implementation of the model, the strain increment is the total strain from the last load reversal, thus the total secant modulus is used. The total equivalent uniaxial strain is defined as the integral of the incremental strains $d\varepsilon_{ui}$:

$$\varepsilon_{ui} = \int d\varepsilon_{ui} \quad (6)$$

In practical applications, the infinitesimal increment $d\varepsilon_{ui}$ is substituted by a finite increment $\Delta\varepsilon_{ui}$, and $\varepsilon_{ui} = \sum \Delta\varepsilon_{ui}$.

It is important to note that neither incremental nor

total equivalent uniaxial strains transform in the same manner as real strains. They are fictitious strains defined in the current principal stress directions. If Eqs. (1) and (5) are compared, the equivalent uniaxial strain increments $d\epsilon_{ui}$ can then be related to the true strain increments in the current orthotropic axes [7,1]. Eq. (1) can be rewritten in the form:

$$\begin{Bmatrix} d\sigma_1 \\ d\sigma_2 \\ d\sigma_3 \end{Bmatrix} = \mathbf{E}\mathbf{H} \begin{Bmatrix} d\epsilon_1 \\ d\epsilon_2 \\ d\epsilon_3 \end{Bmatrix} \quad (7)$$

or

$$\begin{Bmatrix} d\sigma_1 \\ d\sigma_2 \\ d\sigma_3 \end{Bmatrix} = \mathbf{E} \begin{Bmatrix} d\epsilon_{u1} \\ d\epsilon_{u2} \\ d\epsilon_{u3} \end{Bmatrix} \quad (8)$$

with:

$$\mathbf{E} = \begin{bmatrix} E_1 & 0 & 0 \\ 0 & E_2 & 0 \\ 0 & 0 & E_3 \end{bmatrix}$$

$$\mathbf{H} = \begin{bmatrix} (1-v_{23}v_{32})/\Omega & (v_{21}+v_{23}v_{31})/\Omega & (v_{31}+v_{21}v_{32})/\Omega \\ (v_{12}+v_{13}v_{32})/\Omega & (1-v_{13}v_{31})/\Omega & (v_{32}+v_{12}v_{31})/\Omega \\ (v_{13}+v_{12}v_{23})/\Omega & (v_{23}+v_{13}v_{21})/\Omega & (1-v_{12}v_{21})/\Omega \end{bmatrix}$$

$$\begin{Bmatrix} d\epsilon_{u1} \\ d\epsilon_{u2} \\ d\epsilon_{u3} \end{Bmatrix} = \mathbf{H} \begin{Bmatrix} d\epsilon_1 \\ d\epsilon_2 \\ d\epsilon_3 \end{Bmatrix}$$

Even though the above definition of the equivalent uniaxial strain increments is often used for theoretical purposes in presenting the concept of equivalent uniaxial strains, the equivalent uniaxial strains are typically computed based on Eq. (5).

4. Ultimate strength surfaces and current material strength

As previously discussed, the uniaxial stress–strain curves are used to define the current material properties, in particular the current stresses and the material moduli. The stress–strain curves are functions of the peak stresses f_{ci} and the corresponding strains ϵ_{ci} , where the subscript i indicates the three principal stress directions. f_{ci} and ϵ_{ci} are defined by two ultimate envelopes, one in the principal stress space, the other in the equivalent uniaxial strain space. The ultimate stress and strain surfaces, as well the procedure to determine the current peak stress and the corresponding strains are discussed hereafter.

The ultimate stress surface defines the ultimate stress values f_{c1}, f_{c2}, f_{c3} for a given principal stress ratio $\sigma_{P1}/\sigma_{P2}/\sigma_{P3}$. These are not failure points, but rather combinations of maximum stress values. The ultimate stress surface of concrete used in this work is a modification of the five-parameter surface of Willam and Warnke [21]. The modified surface is shown in Fig. 1 and is described by the following equation:

$$\tau_0^2 + A \left(\frac{\tau_0}{\sqrt{2}} r(e, \varphi) + \sigma_0 \right) + B = 0 \quad (9)$$

where $r(e, \varphi)$ is the polar radius as defined by Menetrey and Willam [14]:

$$r(e, \varphi) = \frac{a\eta^2 + b^2}{a\eta + b\sqrt{a(\eta^2 - 1) + b^2}} \quad (10)$$

with

$$A = \frac{f_c^2 - f_t^2}{9f_c} (2 + \alpha); \quad B = -\frac{2f_c f_t}{9}$$

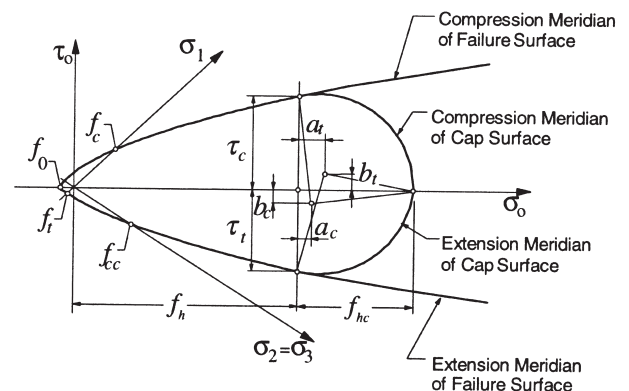


Fig. 1. Concrete ultimate surface with cap model in the Rendulic plane.

and where $\alpha=f_t/f_c$ is the material brittleness, f_c, f_t are the uniaxial compression and tensile strength, respectively, and $a=1-e^2, b=2e-1, \eta=2 \cos(\varphi)$. $\varphi=\frac{1}{3} \arccos[(3\sqrt{3}/2)(J_3/(J_2)^{3/2})]$ is the Lode angle of orientation of the stress-point in the deviatoric plane with J_2 and J_3 being the second and third invariant of the deviatoric stress tensor. e is the eccentricity [14] that defines the out-of roundness of the deviatoric section of the failure surface and is expressed in terms of the material brittleness α as:

$$e = \frac{2+\alpha}{4-\alpha} \tag{11}$$

The polar radius in Eq. (10) defines the form of the ultimate surface in the deviatoric plane $\sigma_0=\text{const}$. For $0.5 \leq e \leq 1.0$ it describes a smooth convex (elliptical) curve, as depicted in Fig. 1.

The compression ($\varphi=60^\circ$) and the extension ($\varphi=0^\circ$) meridians of the ultimate surface are shown in Fig. 1 on the Rendulic plane. These sections are parabolic curves, which pass through a set of characteristic points, namely the points of uniaxial compression and tensile strength (f_c, f_t , respectively), the point of biaxial compression strength (defined as $f_{cc}=\frac{f_c}{4}[(1-\alpha^2)+\sqrt{(1-\alpha^2)^2+16}]$), and the point of equi-triaxial extension (defined as $f_0=-B/A=2f_t/[(1-\alpha^2)(2+\alpha)]$).

In order to account for the material strain hardening and the strength limits under tri-axial compression, a cap surface is introduced, that is described by the following equation:

$$\tau(\sigma_0, \varphi) = \tau_c \frac{1}{\bar{r}(e, \varphi)} \tag{12}$$

where $\bar{r}(e, \varphi)$ is the polar radius defined by Eq. (10), with e being the eccentricity $e=\tau_t/\tau_c$. The parameters τ_c and τ_t represent the interceptions between the cap surface and the compression ($\varphi=60^\circ$) and the tension ($\varphi=0^\circ$) meridians, respectively (Fig. 1). These curves are functions of the hydrostatic stress and are defined by the following quadratic equations:

$$\left. \begin{aligned} \tau_c &= \{ [(\tau_c^c + b_c)^2 + a_c^2] - [\sigma_0 + (f_h + a_c)]^2 \}^{\frac{1}{2}} - b_c \\ \tau_t &= \{ [(\tau_t^c + b_t)^2 + a_t^2] - [\sigma_0 + (f_h + a_t)]^2 \}^{\frac{1}{2}} - b_t \end{aligned} \right\} \tag{13}$$

where

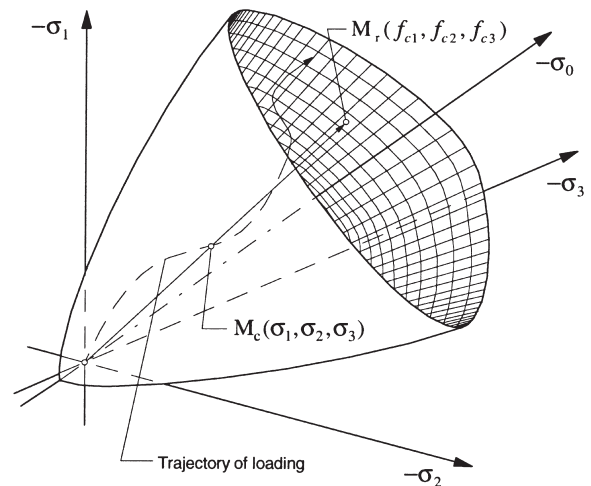
$$b_c = \frac{f_{hc}^2 - 2\tau_c^c f_{hc} k_c - \tau_c^{c^2}}{2(f_{hc} k_c + \tau_c^c)}, \quad a_c = (\tau_c^c + b_c) k_c$$

f_h is the hydrostatic pressure at which the cap surface touches the failure surface, f_{hc} is the parameter specified in Fig. 1, τ_c^c, τ_t^c are the octahedral shear stresses at the points where the cap compression and tension meridians, respectively, touch the corresponding failure surface

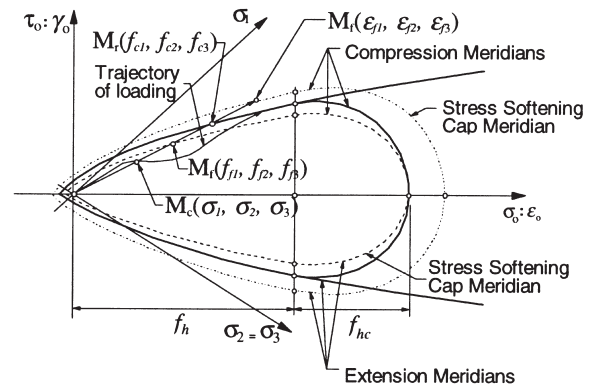
meridians and k_c, k_t are the slopes of the failure surface compression and tension meridians, respectively, at the point where the cap surface touches the failure surface. Fig. 1 shows the compression and extension meridians of the cap surface as well as the parameters that appear in the definitions of Eq. (13).

The determination of the current concrete strength values f_{c1}, f_{c2} and f_{c3} is based on the ultimate strength surface in Eq. (9) and is defined as follows. If a point $M_c(\sigma_1, \sigma_2, \sigma_3)$ on the loading trajectory in principal stress space represents the current stress state of the material in Fig. 2(a), then a line that extends from the origin through the current stress point penetrates the ultimate strength surface at point $M_r(f_{c1}, f_{c2}, f_{c3})$. When loading reversal takes place, the origin is shifted to the point defined by the three principal stresses at the point of reversal.

In a similar manner, the ultimate surface in the equivalent uniaxial strain space $\epsilon_{u1}, \epsilon_{u2}$ and ϵ_{u3} is used for the



a) Strength Parameters



b) Softening Parameters

Fig. 2. Definition of current material strength and softening parameters.

determination of the current ultimate equivalent uniaxial strains ϵ_{c1} , ϵ_{c2} and ϵ_{c3} . It is postulated that there is a surface in the equivalent uniaxial strain space that has the same shape as the ultimate strength surface [5,7]. This surface is based on Eq. (9), where σ_0 is substituted by $\epsilon_0=(\epsilon_{u1}+\epsilon_{u2}+\epsilon_{u3})/3$, τ_0 by $\gamma_0=[(\epsilon_{u1}-\epsilon_{u2})^2+(\epsilon_{u2}-\epsilon_{u3})^2+(\epsilon_{u3}-\epsilon_{u1})^2]^{1/2}/3$, f_c by ϵ_c and f_t by ϵ_t .

5. Uniaxial stress–strain envelopes

The concrete constitutive laws based on the equivalent uniaxial strain concept proposed to date use the uniaxial constitutive law proposed by Saenz [16] to describe the response of concrete in compression. This curve is very convenient because a unique equation describes both the ascending and the post-peak softening response. The law is defined by the initial stiffness E_0 , the peak point ϵ_c , f_c and a post-peak point ϵ_r , f_r that determines how rapidly the material softens. The constitutive equation is:

$$\sigma = f_c \frac{K \left(\frac{\epsilon}{\epsilon_c} \right)}{1 + A \left(\frac{\epsilon}{\epsilon_c} \right) + B \left(\frac{\epsilon}{\epsilon_c} \right)^2 + C \left(\frac{\epsilon}{\epsilon_c} \right)^3} \quad (14)$$

where the following notation is used

$$K = E_0 \frac{\epsilon_c}{f_c} \quad K_\epsilon = \frac{\epsilon_r}{\epsilon_c} \quad K_\sigma = \frac{f_r}{f_c}$$

$$A = C + K - 2 \quad B = 1 - 2C \quad C = K \frac{(K_\sigma - 1)}{(K_\epsilon - 1)^2} - \frac{1}{K_\epsilon}$$

Eq. (14), however, works well only if $E_0/E_c \geq 2$ (where $E_c = f_c/\epsilon_c$), that is when the secant modulus at the peak point is no larger than half the initial modulus E_0 . If this condition is not satisfied, then the curve has a double curvature between the origin and the peak point, that causes the material stiffness to initially increase before returning to E_0 and eventually decreasing. This problem can be partially corrected [4] by freezing E_0/E_c to a maximum value of 2, independently of the actual modulus ratio.

In the present work a different approach is followed. Two curves are used to describe the material response in uniaxial compression. The curve proposed by Popovics [15] describes the ascending branch up to the peak point, while the curve of Saenz [16] is used for the post-peak response. This approach avoids any limitation in the curve definition, while retaining the continuity and smoothness of the response in the pre- and post-peak ranges. Popovics' curve is defined by the following equation:

$$\sigma = f_c \frac{K \left(\frac{\epsilon}{\epsilon_c} \right)}{1 + (K-1) \left(\frac{\epsilon}{\epsilon_c} \right)^r} \quad (15)$$

where the exponent $r = K/K - 1$.

Eqs. (14) and (15) define the material response in uniaxial compression. Similar equations are defined in tension, with initial stiffness E_0 and peak point ϵ_t , f_t . The monotonic compression and tension envelopes are shown in Fig. 3.

The uniaxial law is used to compute the material response in the three principal stresses–equivalent uniaxial strains directions. The values of the peak points ϵ_{ci} , f_{ci} ($i=1, 2, 3$) are computed from the ultimate strength curves previously defined, based on the current principal stress and equivalent uniaxial strain ratios. On the other hand, the definition of points ϵ_{ti} , f_{ti} that control the post-peak response of the stress–strain envelope is not possible on a rigorous experimental base because of the test-dependency of the post-peak branch [7,20,9]. However, instead of the approach by Balan et al. [1], the stress f_r of the post peak point is assumed to depend on f_c , which increases with the level of lateral confinement. Based on a number of experimental results, the following expression was implemented:

$$\epsilon_r = 4\epsilon_c, \quad f_r = f_c \left(5 - \frac{f_c}{f'_c} \right) \frac{f_c}{f'_c} \leq 4.3 \quad (16)$$

The above equation models the experimentally observed shift from brittle to ductile behavior in axially loaded specimens under increasing lateral confinement.

6. Poisson ratio

The definition of the transverse strain ratios ν_{ij} in Eq. (2) is an important step in the formulation of the concrete law. It is typically assumed [5] that Poisson's ratio ν for

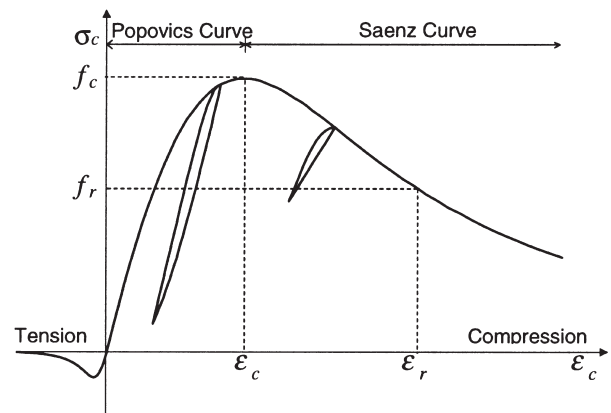


Fig. 3. Monotonic uniaxial strain curve in tension and compression.

concrete ranges between 0.15 and 0.22. However, it has been experimentally observed that the apparent Poisson's ratio is constant only for uniaxial stresses smaller than approximately 80% f'_c . As the peak strength is approached, Poisson's ratio increases and becomes even larger than 0.5 in the crushing phase. This dilatancy phenomenon is due to the growth of unstable micro cracks near and after the peak stress.

The following expression is used in the proposed constitutive law to define the transverse strain ratios:

$$v_{ij} = \sqrt{v_{ui}v_{uj} \frac{E_i}{E_j}} \quad (17)$$

where v_{ui} is the uniaxial transverse strain ratio in the direction i . The above definition of v_{ui} guarantees symmetry of C_0 in Eq. (2). The following expression is used to define v_{ui} :

$$v_{ui} = v_0 \left[1 + \frac{1}{K_v} \left\{ A_i \left(\frac{\varepsilon_{ui}}{\varepsilon_{ci}} \right) + B_i \left(\frac{\varepsilon_{ui}}{\varepsilon_{ci}} \right)^2 + C_i \left(\frac{\varepsilon_{ui}}{\varepsilon_{ci}} \right)^3 \right\} \right] \quad (18)$$

where v_0 is the initial Poisson's ratio, A_i , B_i , C_i are the same parameters as used in Eq. (14) with $K_f=1/2v_0$ and K_v defined as:

$$K_v = \frac{E_0 \varepsilon_{ci}}{2f_{ci}}$$

Eq. (18) is similar to the cubic expression defined by Elwi and Murray [7] and later used by Balan et al. [1]. The K_v coefficient has been added here to prevent Ω in Eq. (2) from approaching a zero value or becoming negative. The limit value of $\Omega=0$ describes an incompressible material and creates serious numerical problems in the finite element implementation of the constitutive law.

7. Cyclic behavior

The complete implementation of the proposed constitutive law necessitates the definition of the cyclic behavior under an arbitrary load history. Following Balan et al. [1] the loading/unloading criterion is based on the definition of the following loading function:

$$f = \sqrt{\frac{\varepsilon_{u1}^2 + \varepsilon_{u2}^2 + \varepsilon_{u3}^2}{\varepsilon_{c1}^2 + \varepsilon_{c2}^2 + \varepsilon_{c3}^2}} \quad (19)$$

where ε_{ui} and ε_{ci} are the equivalent uniaxial strains and ultimate strains, respectively. If f_{\max} is the maximum value of the loading function up to the current load step, the loading and unloading conditions are:

$$f > f_{\max} \text{ loading}$$

$$f \leq f_{\max} \text{ unloading}$$

The above loading and unloading conditions complete

the definition of the constitutive law. Unlike the law presented by Balan et al. [1] no special rules have to be established to define the material post-peak behavior after compression crushing or the post-peak behavior after cracking in tension. The expression for C_0 in Eq. (2) is used for any loading or reloading conditions, using the current material parameters derived from the uniaxial constitutive laws in the principal stress directions. This leads to a much simpler numerical implementation of the material model and avoids some of the numerical convergence problems encountered with the original model [1], in particular under non-proportional loading conditions. Every time unloading takes place, the origin of the incremental law is shifted to the last reversal point.

8. Behavior of 3D constitutive law

The 3D constitutive law has been implemented in the finite element program FEAP [19] as a stand-alone routine (driven by a material driver that allows both stress, strain and mixed loading) and is commonly used for solid finite elements. The constitutive law is entirely based on the de-coupling of the principal stresses and equivalent uniaxial strains. The major difference with the model previously presented by Balan et al. [1] is that no special provision is taken for post-peak behavior after crushing in compression or cracking in tension. The continuous equivalent uniaxial laws entirely govern the material response, based on the incremental secant constitutive law given by Eq. (2). The principal stress axes are allowed to rotate and are not coaxial with the principal strains. Bouzaiene and Massicotte [4] (who assume that the axes of orthotropy are parallel to the principal strain axes) comment on the numerical advantages of assuming the axes of orthotropy to be parallel to the principal directions (either stress or strain). Arbitrarily oriented orthotropic axes would greatly complicate the formulation of the constitutive law, whose main advantage is indeed its simplicity and conciseness.

Some authors have argued that orthotropic models are not invariant. This implies that the same load history applied under a different set of reference axes would yield different results, in particular different principal strains and different strain directions. This possible shortcoming is discussed at length in Bazant [3], where specific examples are presented to illustrate the lack of invariance. Bazant [3] asserts that only when the principal stresses are parallel to the principal strains (which leads to a unique expression of the shear moduli) is the model tensorially invariant and hence fully consistent. Bouzaiene and Massicotte [4] follow this approach.

The authors have reproduced the same examples of Bazant [3] and several more and have found that the model proposed in this study is tensorially invariant and hence fully consistent. The main reason for the consist-

ency of the proposed orthotropic model lies in the fact that even though the model is incremental, the total secant form of the material matrix \mathbf{C}_0 is used in the constitutive law of Eq. (1). Also, the transformation matrix \mathbf{T} in Eq. (4) is the rotation matrix between the current orthotropic axes and the total reference system. With the proposed model, consistent stress and strain rotations lead to identical results, independently of the set of reference axes, for applied stresses of different magnitude up to the peak response.

9. Model verification

To establish the validity of the material model, correlation studies between analytical results and experimental tests are presented hereafter for concrete specimens under triaxial loading conditions. All the results were obtained using the finite element program FEAP [19]. Some of the results were obtained with an eight-node brick element, others using a constitutive driver for 3D constitutive laws that can apply stress-, strain- and mixed-control loading histories.

The first application is a series of uniaxial tests under constant lateral confinement conducted at the University of Colorado, Boulder [18]. The main scope of these tests was to show the transition of the concrete behavior from brittle-softening to ductile-hardening as the lateral confinement increases. The experimental and analytical results in the vertical loading direction are shown in Fig. 4. The unconfined material properties used for the analyses were $f_c=5.0$ ksi, $f_t=0.5$ ksi, $E_0=2400$ ksi, $\nu_0=0.2$, $\epsilon_c=0.004$, $\epsilon_t=0.0002$. The values of σ_{lat} , the constant lateral compressive stress, are indicated, for the different tests in Fig. 4. The above-mentioned transition between brittle and ductile is clear in both experimental and analytical results. In order to obtain good correlation with the original results by Smith et al. [18] two aspects of the constitutive law must be carefully selected. One is

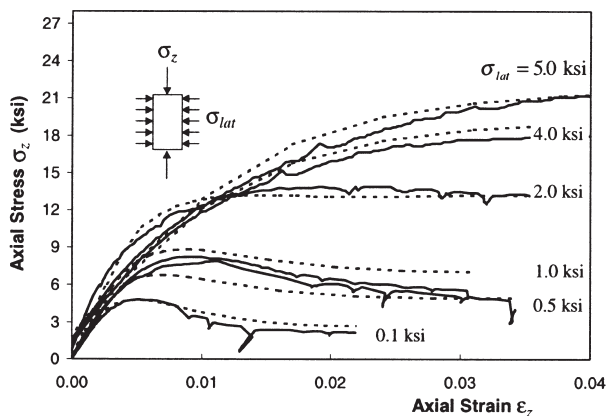


Fig. 4. Monotonic confined compression tests by Smith et al. [18].

the cap model, the other the post-peak behavior parameters. As the lateral confinement increases, the loading direction moves closer to the hydrostatic axis, thus the ultimate strength concrete parameter used in the equivalent uniaxial laws are selected from the cap surface. As for the post-peak behavior, this is governed by the position of point ϵ_r, f_r in Fig. 3. This point, fixed in the original work by Balan et al. [1], is a function of the peak stress f_c according to the formula of Eq. (16).

Hurlbut [8] extended the work by Smith et al. [18] to cyclic confined compression tests. The experimental and analytical results for three different tests are shown in Fig. 5. The three cases refer to different levels of lateral confinement, $\sigma_{lat}=0, 0.1$ and 1 ksi, respectively. The unconfined concrete material properties used for the analyses were $f_c=2.77$ ksi, $f_t=0.28$ ksi, $E_0=2400$ ksi, $\nu_0=0.2$, $\epsilon_c=0.00235$, $\epsilon_t=0.00014$. The correlation between analytical and experimental results is good. The model is able to represent the changes in peak stress and strain and the effects of confinement in the post-peak range. The adopted scheme for unloading and reloading also leads to good correlation in the partial unloading–reloading cycles. Some of the discrepancies in the results are due to the procedure followed in the numerical tests. Mixed control was used to trace the stress histories, with imposed axial displacements and constant lateral confining stresses. Fig. 6 shows the experimental and analytical results for the biaxial compression tests conducted by van Mier [20]. This is a case of proportional biaxial loading, with $\sigma_3=0$ and $\sigma_1/\sigma_2=10$. The material properties used for the analyses were $f_c=7.2$ ksi, $f_t=0.5$ ksi, $E_0=3700$ ksi, $\nu_0=0.2$, $\epsilon_c=0.0034$, $\epsilon_t=0.0002$. Experimental and analytical results match well, especially in the loading direction ϵ_1, σ_1 . The discrepancy in the unconfined direction 3 is due to the limit value of the Poisson ratio. In order to assure numerical convergence, ν is limited to 0.5 , while experimental results show values of the apparent Poisson ratio larger than 1 , due to the opening of large vertical cracks [12]. Furthermore, the experimental results show a somewhat puzzling response in direction 3 for low stresses. The specimen first appears to contract in the unconfined direction 3, and then changes this tendency and starts expanding very rapidly. This seems to indicate a measurement error or other boundary effects that cannot be captured by the analytical model.

Finally, an example of triaxial non-proportional loading is presented. This is an important test, since the most demanding stress histories in concrete analyses are those with non-proportional loading. The test results are part of the extensive experimental results conducted at the University of Colorado, Boulder by Scavuzzo et al. [17]. The material properties used for the analyses were $f_c=3.5$ ksi, $f_t=0.3$ ksi, $E_0=3500$ ksi, $\nu_0=0.2$, $\epsilon_c=0.00215$, $\epsilon_t=0.0002$. Fig. 7(a) shows the loading path in the principal stress space as a function of the applied loading step. The specimen was first loaded along the hydrostatic axis

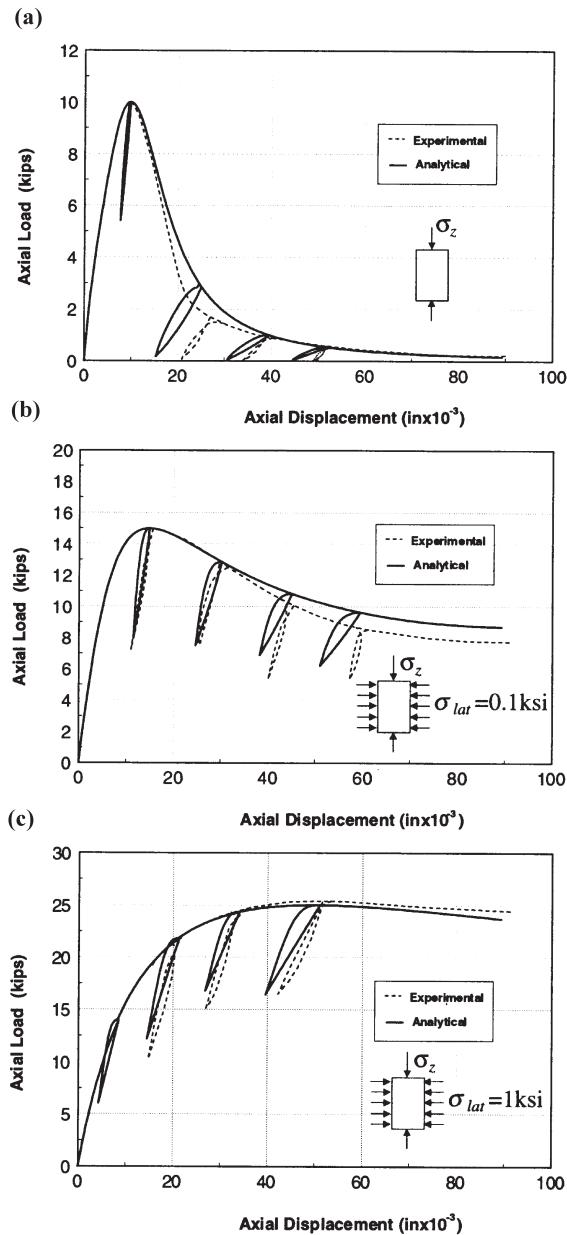


Fig. 5. Cyclic confined compression tests by Hurlbut [8]: (a) load–displacement response for compression without confining pressure; (b) load–displacement response for compression with 100 psi confining pressure; (c) load–displacement response for compression with 1000 psi confining pressure.

up to $\sigma_0 = -6$ ksi. The stresses were then modified by cyclic loading on the corresponding deviatoric plane. The results are illustrated in Fig. 7(b–d). The correlation between experimental and analytical results is good even for such a complex loading history. The analytical results were obtained using stress-control, and since the specimen shows an almost perfectly plastic response, the response is very sensitive to even small stress changes. This explains the difference in strain prediction between analytical and experimental results.

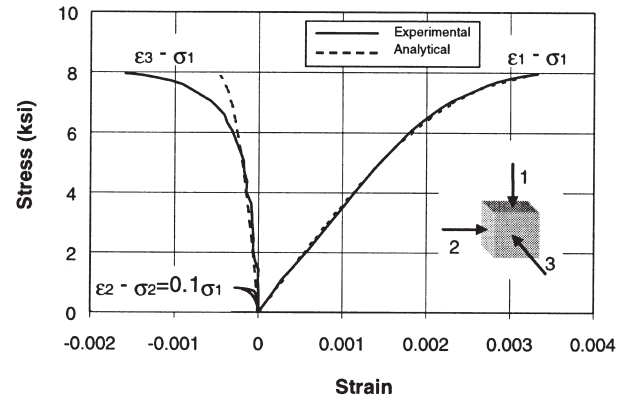


Fig. 6. Biaxial test by van Mier [20].

10. Conclusions

The general formulation of a three-dimensional material model for the nonlinear finite element analysis of concrete structures under short term, cyclic, non-proportional loads is presented in this paper. The law is an orthotropic model with the axes of orthotropy parallel to the principal stress directions. Principal stress and principal strain directions are not parallel. The model builds on the concept of equivalent uniaxial strains first proposed in Darwin and Pecknold [6] and Bashur and Darwin [2]. Ultimate strength and strain surfaces are used in the principal stress and equivalent uniaxial strain spaces to find the material characteristics of the principal stress–equivalent uniaxial strain curves. The ultimate surface is that proposed by Willam and Warnke [21], with a cap surface added to account for loading along or near the hydrostatic axis.

The model is general and can describe monotonic and cyclic loading, as well as proportional and non-proportional loads. Post-peak crushing in compression and cracking in tension are included. Furthermore, the model accounts for the transition between brittle-softening to ductile-hardening response in compression under increasing lateral confinement. The cyclic behavior is described by shifting the loading curve to the last inversion point. The model has been successfully implemented in the finite element code FEAP [19] as a constitutive model driven by either finite elements or by a constitutive driver that allows different mixed control techniques to be applied, including shear stresses and strains.

Correlation studies with available experimental tests show very good predictions with the numerical model. Satisfactory responses are observed under monotonic, cyclic, proportional and non-proportional load cases. The model simplicity makes it particularly attractive for the study of reinforced concrete sub-assemblages where numerical efficiency is important to minimize computational costs.

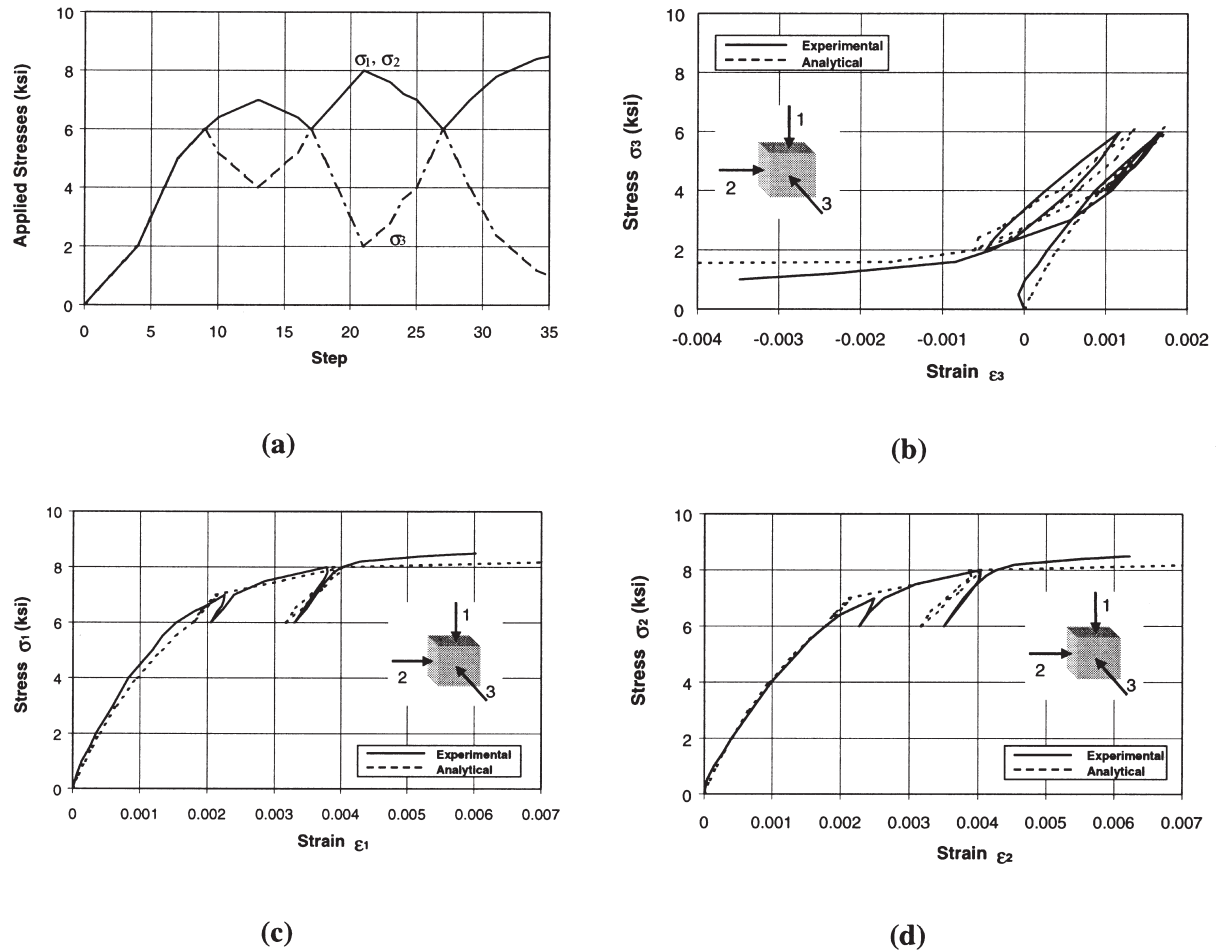


Fig. 7. Cyclic triaxial compression tests by Scavuzzo et al. [17]: (a) applied stress histories; (b) response in direction 3; (c) response in direction 1; (d) response in direction 2.

Acknowledgements

This work is partially supported by the National Science Foundation under Grant No. CMS-9804613. This support is gratefully acknowledged. However, opinions expressed in this paper are those of the authors and do not necessarily reflect those of the sponsor. The help from Professors K. Gerstle and K.J. Willam of the Department of Civil, Environmental and Architectural Engineering of the University of Colorado, Boulder, in locating useful experimental data is gratefully acknowledged.

References

- [1] Balan TA, Filippou FC, Popov EP. Constitutive model for 3D cyclic analysis of concrete structures. *J Engng Mech, ASCE* 1997;123(2):143–53.
- [2] Bashur FK, Darwin D. Nonlinear biaxial law for concrete. *J Struct Div, ASCE* 1978;104(1):157–70.
- [3] Bazant ZP. Comment on orthotropic models for concrete and geomaterials. *J Engng Mech, ASCE* 1983;109(3):849–65.
- [4] Bouzaiene A, Massicotte B. Hypoelastic tridimensional model for nonproportional loading of plain concrete. *J Engng Mech, ASCE* 1997;123(11):1111–20.
- [5] Chen WF. *Plasticity in reinforced concrete*. New York: McGraw-Hill, 1982.
- [6] Darwin D, Pecknold DA. Nonlinear biaxial stress–strain law for concrete. *J Engng Mech, ASCE* 1977;103(2):229–41.
- [7] Elwi AA, Murray DW. A 3D hypoelastic concrete constitutive relationship. *J Engng Mech, ASCE* 1979;105(4):623–41.
- [8] Hurlbut BJ. Experimental and computational investigation of strain softening in concrete. Report AFOSR 80-0273. US Air Force Office of Scientific Research, University of Colorado, Boulder, 1985.
- [9] Jansen DC, Shah SP, Rossow EC. Stress–strain results of concrete from circumferential strain feedback control testing. *ACI Journal* 1995;92(6):419–28.
- [10] Kang HD, Spacone E, Willam KJ. A study of compressive failure in over-reinforced concrete beams. In: FRAMCOS-3, Oct 12–16; Gifu, Japan, vol. 2, 1998:1195–210.
- [11] Kolymbas D. An outline of hypoplasticity. *Arch Appl Mech* 1991;61:143–51.
- [12] Kupfer HB, Hilsdorf HK, Rüschi H. Behavior of concrete under biaxial stresses. *ACI Journal* 1969;66(8):656–66.
- [13] Lekhnitskii SG. In: Brandstatter JJ, editor. *Theory of elasticity of an anisotropic elastic body*. San Francisco, CA: Holden Day, Inc., 1963.

- [14] Menetrey P, Willam KJ. Triaxial failure criterion for concrete and its generalization. *ACI Structural Journal* 1995;92(3):311–8.
- [15] Popovics S. Numerical approach to the complete stress–strain relation for concrete. *Cement Concrete Res* 1973;3(5):583–99.
- [16] Saenz IP. Discussion of ‘equation for the stress–strain curve of concrete, by P. Desay and S. Krishan’. *ACI Journal* 1964;61(9):1229–35.
- [17] Scavuzzo R, Stancowski T, Gerstle K, Ko H-Y. Stress–strain curves for concrete under multiaxial load histories. NSF CME 80-01508. Department of CEAE, University of Colorado, Boulder, 1983.
- [18] Smith SS, Willam KJ, Gerstle KH, Sture S. Concrete over the top, or: is there life after peak? *ACI Journal* 1989;86(5):491–7.
- [19] Taylor RL. FEAP user manual, v7.1. Berkeley, CA: Department of Civil and Environmental Engineering, University of California, 1999.
- [20] van Mier JGM. Strain-softening of concrete under multiaxial loading conditions. PhD thesis, Eindhoven University of Technology, Eindhoven, The Netherlands, 1984.
- [21] Willam KJ, Warnke EP. Constitutive model for the triaxial behavior of concrete. *Int Assoc Bridge Struct Engng Proc* 1975;19:1–30.
- [22] Willam KJ, Hurlbut B, Sture S. Experimental and constitutive aspects of concrete failure. In: Meyer, Okamura, editors. *Finite element analysis of reinforced concrete structures*. New York: ASCE, 1986.